

Section S1. Theoretical calculation for local octahedral distortions

In this section, we evaluated the incorporated AlO₆ octahedral distortions among TiO₂ and SiO₂ polymorphs, based on the first-principles calculation. The geometry optimization was conducted using the Cambridge Serial Total Energy Package (CASTEP) program within the Material Studio software (Clark et al. 2005), and the calculations were carried out on the basis of the SCAN (meta-generalized-gradient approximation) meta-GGA functional and the BFGS (Broyden-Fletcher-Goldfarb-Shanno) algorithm. Totally 96 atoms (32 TiO₂ formulae) were included in the models, corresponding to 2×2×4 and 2×2×2 supercells in the CaCl₂- and α -PbO₂-type structures. Only one Ti⁴⁺ cation in a supercell was replaced by Al³⁺ (Fe³⁺), resulting in a 3.1 mol.% concentration in the hosts of CaCl₂-TiO₂, α -PbO₂-TiO₂, as well as rutile-SiO₂ (stishovite) and CaCl₂-SiO₂ (poststishovite).

Sampling of the First Brillouin zone was achieved using 3×3×3 *k* meshes (Blöchl et al. 1994). Ultrasoft pseudopotentials were employed to model the relationship between core and valence electrons. (Kresse and Joubert 1999). The valence electron configurations used in our calculations were 3*d*²4*s*², 3*s*²3*p*¹, 3*s*²3*p*², 2*s*²2*p*⁴ and 3*d*⁶4*s*² for Ti, Al, Si, O and Fe, respectively. A cutoff energy of 400 eV was employed in our calculations. Convergence criteria were set at 5×10⁻⁶eV/atom, 0.01eV/Å, 0.02 GPa, and 5×10⁻⁴Å for energy, maximum force, maximum displacement, respectively. The calculated M³⁺-O²⁻ bond lengths and M³⁺O₆-octahedral quadratic elongations in various TiO₂ and SiO₂ hosts are listed in **Supplemental Table S3**.

References

- Blöchl, P.E., Jepsen, O., and Andersen, O.K. (1994) Improved tetrahedron method for Brillouin-zone integrations. *Physical Review B*, 49, 16223-16233. <https://doi.org/10.1103/PhysRevB.49.16223>.
- Clark, S.J., Segall, M.D., Pickard, C.J., Hasnip, P.J., Probert, M.J., Refson, K., and Payne, M.C. (2005) First principles methods using CASTEP. *Zeitschrift Fur Kristallographie*, 220, 567-570. <https://doi.org/10.1524/zkri.220.5.567.65075>.
- Kresse, G. and Joubert, D. (1999) From ultrasoft pseudopotentials to the projector augmented-wave method. *Physical Review B*, 59, 1758-1775. <https://doi.org/10.1103/PhysRevB.59.1758>.

Table S1. Compositions of Synthetic samples from electron microprobe analyses.

		Rutile-type	CaCl ₂ -type		α -PbO ₂ -type	
		Ti _{0.998} Al _{0.002} O ₂	Ti _{0.961} Al _{0.053} O ₂	Ti _{0.972} Al _{0.037} O ₂	Ti _{0.957} (AlH) _{0.043} O ₂	Ti _{0.930} (AlH) _{0.070} O ₂
<i>wt %</i>	TiO ₂	99.9(6)	96.1(5)	97.2(3)	96.7(6)	94.7(6)
	Al ₂ O ₃	0.14(2)	3.36(5)	2.3(1)	2.8(4)	4.5(4)
	Total	100.2(5)	99.5(5)	99.5(3)	99.5(6)	99.3(5)
<i>apfu^a</i>	Ti	0.998(6)	0.948(5)	0.963(3)	0.957(6)	0.931(6)
	Al	0.0022 (3)	0.0529(8)	0.037(2)	0.043(6)	0.069(6)

a: abbreviation for atoms per formula unit

Table S2. Atomic anisotropic displacement parameters (Å²) from the single-crystal structure refinements.

		Rutile-type		CaCl ₂ -type		α-PbO ₂ -type		
		Ti _{0.998} Al _{0.002} O ₂	Ti _{0.961} Al _{0.053} O ₂	Ti _{0.972} Al _{0.037} O ₂	TiO ₂	Ti _{0.957} (AlH) _{0.043} O ₂	Ti _{0.930} (AlH) _{0.070} O ₂	
Displacement	Ti/Al ^{oct}	<i>U</i> ₁₁	0.01065(19)	0.01176(12)	0.0112(2)	0.00728(17)	0.00730(17)	0.00763(17)
		<i>U</i> ₂₂	0.01065(19)	0.01197(13)	0.0111(2)	0.0075(19)	0.00856(17)	0.00832(16)
		<i>U</i> ₃₃	0.0078(2)	0.00737(12)	0.0069(2)	0.00643(19)	0.00696(17)	0.00764(17)
		<i>U</i> ₁₂	-0.00014(15)	0.00015(7)	-0.00003(10)	0	0	0
		<i>U</i> ₁₃	0	0	0	-0.00025(11)	-0.00036(7)	-0.00039(7)
		<i>U</i> ₂₃	0	0	0	0	0	0
		<i>U</i> _{eq}	0.00971(16)	0.01037(8)	0.00974(15)	0.00709(12)	0.00761(12)	0.00786(11)
	O	<i>U</i> ₁₁	0.0099(4)	0.0092(2)	0.0086(4)	0.0087(4)	0.0077(3)	0.0090(3)

U_{22}	0.0099(4)	0.0086(3)	0.0084(4)	0.0085(4)	0.0087(3)	0.0077(3)
U_{33}	0.0079(5)	0.0062(2)	0.0063(4)	0.0073(4)	0.0068(3)	0.0078(3)
U_{12}	-0.0025(5)	-0.0025(2)	-0.0021(3)	-0.0003(3)	-0.0007(2)	-0.00091(19)
U_{13}	0	0	0	-0.0002(4)	-0.0010(3)	-0.0010(3)
U_{23}	0	0	0	0.0012(4)	0.0006(3)	0.0005(3)
U_{eq}	0.0092(3)	0.00798(12)	0.0078(2)	0.00819(19)	0.00772(16)	0.00815(15)

Table S3. Calculated M³⁺-O²⁻ bond lengths ($l_1 \leq l_2 < l_3$) and quadratic elongation

$\langle \lambda \rangle$ for the local MO₆ octahedra.

M ³⁺	host	l_1 (Å)×2	l_2 (Å)×2	l_3 (Å)×2	l_0 (Å)	$\langle \lambda \rangle$
Al ³⁺	rutile-TiO ₂ [#]	1.893	1.893	1.901	1.895	1.000618
Ga ³⁺	rutile-TiO ₂ [#]	1.980	1.980	1.982	1.980	1.000610
Cr ³⁺	rutile-TiO ₂ [#]	1.899	1.899	1.931	1.909	1.000735
Fe ³⁺	rutile-TiO ₂ [#]	1.895	1.895	1.901	1.896	1.000614
Ti ³⁺	rutile-TiO ₂ [#]	1.960	1.960	1.986	1.968	1.000687
Al ³⁺	CaCl ₂ -TiO ₂	1.897	1.897	1.912	1.901	1.000663
Al ³⁺	α -PbO ₂ -TiO ₂	1.894	1.900	1.964	1.918	1.001545
Fe ³⁺	α -PbO ₂ -TiO ₂	1.828	1.873	1.936	1.8778	1.001850
Al ³⁺	rutile-SiO ₂	1.843	1.843	1.878	1.854	1.001078
Al ³⁺	CaCl ₂ -SiO ₂	1.847	1.847	1.889	1.860	1.001193

[#]: from Wang et al. (2023).

Table S4. The fitted $\partial v_i / \partial T$ (cm⁻¹·K⁻¹) for Raman and OH-stretching bands in the synthetic samples at high temperatures.

Rutile-type		CaCl ₂ -type				α -PbO ₂ -type					
Ti _{0.998} Al _{0.002} O ₂		Ti _{0.961} Al _{0.053} O ₂		Ti _{0.972} Al _{0.037} O ₂		TiO ₂		Ti _{0.957} (AlH) _{0.043} O ₂		Ti _{0.930} (AlH) _{0.070} O ₂	
ν_i	$\partial \nu_i / \partial T$	ν_i	$\partial \nu_i / \partial T$	ν_i	$\partial \nu_i / \partial T$	ν_i	$\partial \nu_i / \partial T$	ν_i	$\partial \nu_i / \partial T$	ν_i	$\partial \nu_i / \partial T$
(cm ⁻¹)	(cm ⁻¹ ·K ⁻¹)	(cm ⁻¹)	(cm ⁻¹ ·K ⁻¹)	(cm ⁻¹)	(cm ⁻¹ ·K ⁻¹)	(cm ⁻¹)	(cm ⁻¹ ·K ⁻¹)	(cm ⁻¹)	(cm ⁻¹ ·K ⁻¹)	(cm ⁻¹)	(cm ⁻¹ ·K ⁻¹)
142	0.0029(4)	119	0.04 (1)	114	0.033(4)	148	-0.003(3)	152	0.004(2)	156	0.004(2)
231	0.042(3)	236	0.063(3)	236	0.0320(2)	170	-0.018(1)	177	-0.015(2)	178	-0.017(2)
439	-0.031(2)	437	-0.031(2)	440	-0.047(1)	282	-0.027(1)	290	-0.025(2)	290	-0.018(3)
608	-0.011(1)	612	-0.013(2)	610	-0.0097(8)	315	-0.014(1)	315	-0.009(1)	319	-0.007(1)
--	--	--	--	--	--	340	-0.006(1)	343	-0.006(1)	--	--
--	--	--	--	--	--	354	-0.019(2)	358	-0.0141(9)	362	-0.0141(9)
--	--	--	--	--	--	425	-0.002(5)	429	-0.029(2)	433	-0.022(1)

Table S5. Pressure dependence of $\partial v_i / \partial P$ (cm⁻¹·GPa⁻¹), for the Raman and OH-stretching peaks in the synthetic samples.

Rutile-type		CaCl ₂ -type		α -PbO ₂ -type					
Ti _{0.998} Al _{0.002} O ₂		Ti _{0.972} Al _{0.037} O ₂		TiO ₂		Ti _{0.957} (AlH) _{0.043} O ₂		Ti _{0.930} (AlH) _{0.070} O ₂	
v_i	$\partial v_i / \partial P$	v_i	$\partial v_i / \partial P$	v_i	$\partial v_i / \partial P$	v_i	$\partial v_i / \partial P$	v_i	$\partial v_i / \partial P$
(cm ⁻¹)	(cm ⁻¹ ·GPa ⁻¹)	(cm ⁻¹)	(cm ⁻¹ ·GPa ⁻¹)	(cm ⁻¹)	(cm ⁻¹ ·GPa ⁻¹)	(cm ⁻¹)	(cm ⁻¹ ·GPa ⁻¹)	(cm ⁻¹)	(cm ⁻¹ ·GPa ⁻¹)
142	-3.2(2)	124	1.0(3)	150	1.4(3)	153	1.6(3)	157	1.8(5)
237	1.8(3)	244	1.5(1)	173	1.0(4)	175	0.3(1)	179	0.63(10)
445	3.3(7)	444	3.1(1)	286	0.7(3)	287	0.7(1)	291	0.6(1)
609	4.3(3)	615	3.46(5)	315	-0.7(4)	316	-0.23(8)	319	-0.51(6)
--	--	--	--	338	0.7(4)	337	1.00(9)	346	0.89(8)
--	--	--	--	356	2.4(4)	359	1.3(1)	362	1.7(2)
--	--	--	--	427	2.4(2)	430	3.2(2)	433	2.7(2)

--	--	--	--	531	4.9(4)	535	4.86(8)	539	3.6(2)
--	--	--	--	570	5.3(3)	570	4.5(1)	570	4.4(3)
--	--	--	--	605	4.7(4)	622	3.7(1)	629	3.8(2)
--	--	--	--	816	4.3(4)	820	3.7(1)	822	3.6(2)
3280	-9(2)	3315	-26(2)	--	--	--	--	2933	-7.8(9)

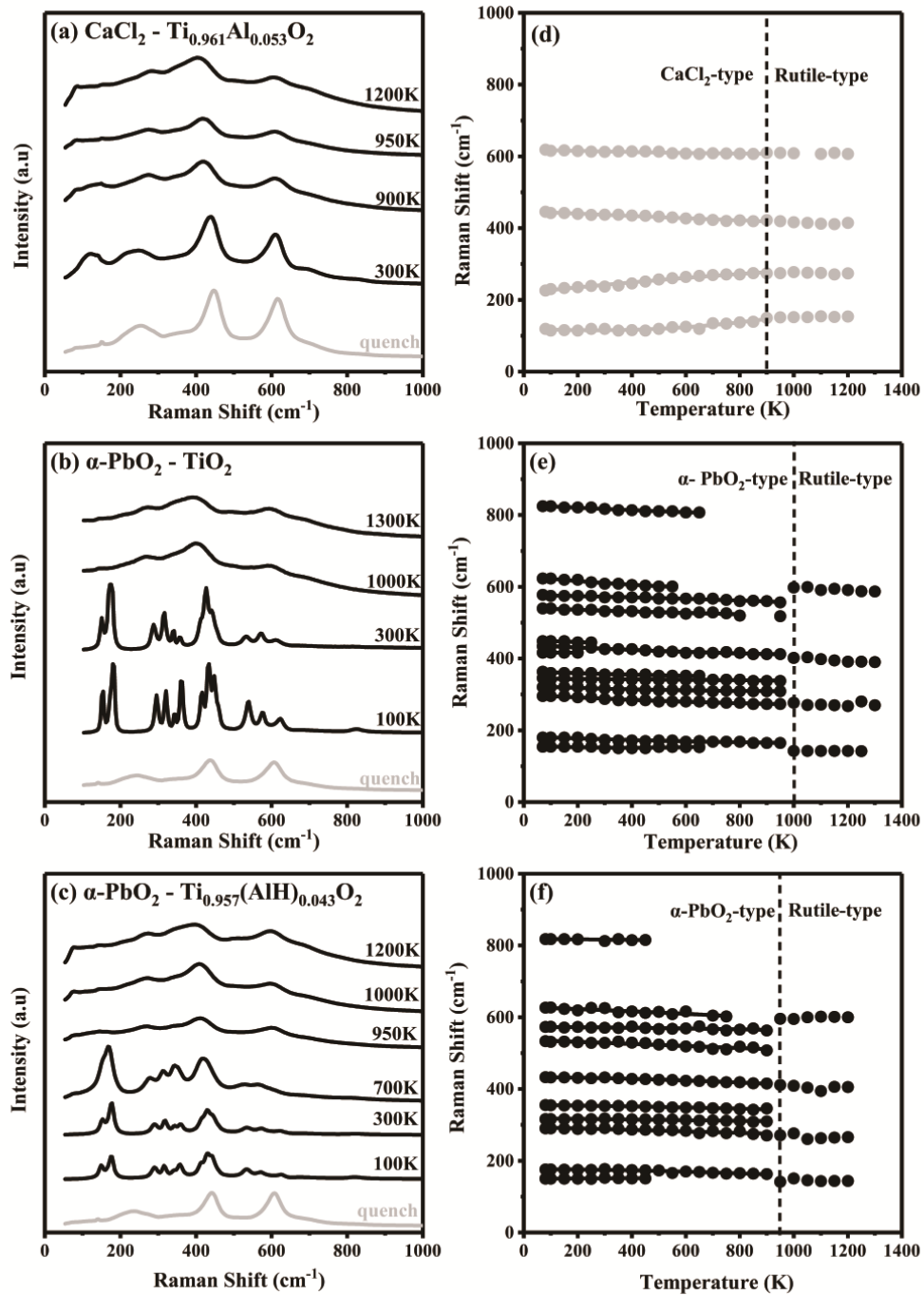


Figure S1

Fig. S1. (a,b,c) Selected Raman spectra at high temperatures and (d,e,f) evolution of the vibrational frequencies with temperature for (a,d) CaCl₂-Ti_{0.961}Al_{0.053}O₂, (b,e) CaCl₂-Ti_{0.961}Al_{0.053}O₂ and (c,f) α-PbO₂-Ti_{0.957}(AlH)_{0.043}O₂. The phase transitions to rutile-type structure around $T = 950$ K are marked as dashed lines in (d,e,f).

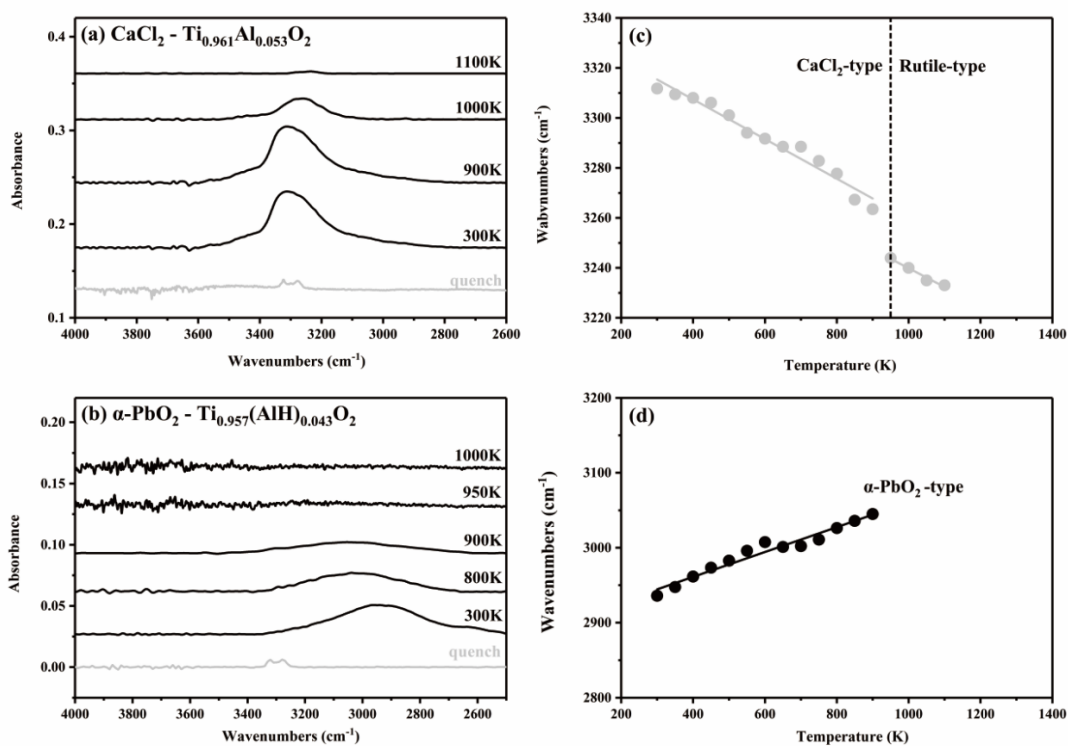


Figure S2

Fig. S2. (a,b) Selected FTIR spectra at high temperatures and (c,d) variation of frequencies with T for the samples of (a,c) $\text{CaCl}_2\text{-Ti}_{0.961}\text{Al}_{0.053}\text{O}_2$ and (b,d) $\alpha\text{-PbO}_2\text{-Ti}_{0.957}(\text{AlH})_{0.043}\text{O}_2$.

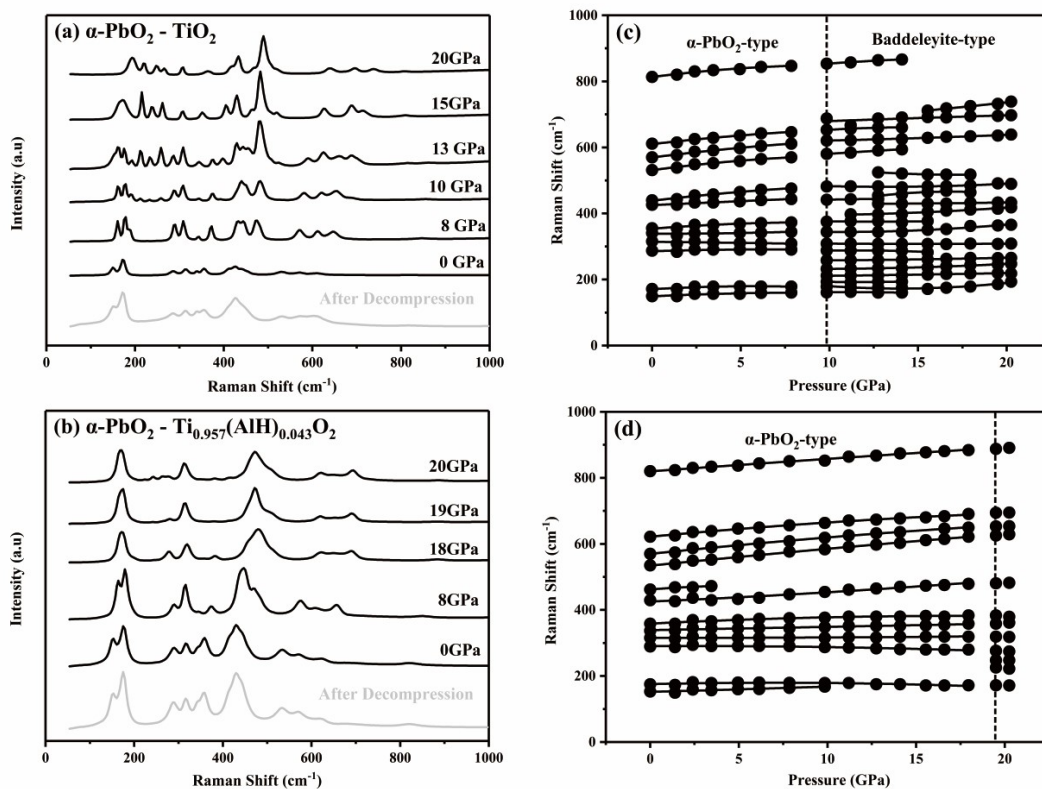


Figure S3

Fig. S3. Representative high-*P* Raman spectra for α -PbO₂-type (a) TiO₂ and (b) Ti_{0.957}(AlH)_{0.043}O₂, and the fitted vibrational frequencies are plotted as a function of pressure in (c,d), respectively.